Hamburger Beiträge
zur Angewandten Mathematik

Microscopic car-following models revisited: From road works to fundamental diagrams

T. Seidel, I. Gasser, and B. Werner

Nr. 2007-16
October 2007

MICROSCOPIC CAR-FOLLOWING MODELS REVISITED: FROM ROAD WORKS TO FUNDAMENTAL DIAGRAMS

T. SEIDEL , I. GASSER , AND B. WERNER

Abstract. We analyse the dynamics of the classical optimal velocity model for the case of inhomogeneous drivers and for the case of road works. We introduce a different viewpoint, the so-called rotation solutions, which in case of an additional symmetry leads to the POM solutions. This approach opens the possibility to analytical and numerical bifurcation studies, which show a big variety in the possible dynamics of this very simple model. In addition we mimic different measurement approaches and recover the inverse greek λ structure in the fundamental diagram.

Key words. traffic flow, numerical bifurcation analysis, Hopf, Neimark-Sacker, bifurcation

AMS subject classifications. 37M20, 65L07, 65P30, 65P40

1. Introduction. In the last decades many authors have studied traffic models for vehicular traffic. There are overview articles on this topic [Hel01, BM00, NWW03, KW04]. The main purpose for these studies is to understand traffic flow phenomena like congestion waves etc. A good understanding opens the possibility to influence or even to control traffic flow.

There is a big variety of mathematical model for traffic flow. The most popular approaches for a certain number of cars on a road are microscopic and macroscopic models. On one side — in the microscopic world — single cars are described, and on the other side — in the macroscopic approach — only spatio-temporal traffic flow quantities like velocity and density are considered.

The two mentioned modelling approaches lead to completely different mathematical models. The microscopic models are represented by cellular automata [SS93], by ordinary differential equations [BHN$^+$95] or by delay differential equations [OWK04]. The macroscopic models are given by systems of nonlinear partial differential equations [LW55, AR00]. As a consequence the mathematical and also the numerical methods used to study such models, may be completely different. However, there are results on the relation between these two modelling appoaches [AKMR02]. In some cases both approaches are used, one for the analysis, the other for the numerics [Gre04].

The microscopic models based on ordinary differential equations or delay differential equations allow a profound understanding of the dynamics of the models. In the last several years various authors have used tools from dynamical systems like bifurcation theory to analyse the global dynamics of such traffic flow models [GSW04]. These techniques were applied to the standard case of N cars on a circular road with (deterministically) prescribed behaviour of each single car. In this case global bifurcation diagrams give the information about stationary or periodic behaviour (for the headways and speeds) and about the corresponding stability of such solutions. Similar results are known for delay differential equation models [OWK04, OS06, OKW05]. These results were all done mainly for the homogeneous case (all cars are equal and the circular road is homogeneous).

When studying non homogeneous cars or situations with road works the methods used right now are limited. In this paper we present a new approach which on one side allows to handle and to understand the global dynamics of models with road works and with inhomogeneous cars, and on the other side throw new light on earlier results in [GSW04]. This approach is based on certain periodic solutions on the circle which

we call *rotation solutions*. In the special case of homogeneous cars these solutions become solutions which — following [AGMP91] — are called Ponies-On-A-Merry-Go-Round-solutions (POMs). In this context Poincaré-type maps gain importance and the viewpoint is shifted to a dynamical system approach in terms of maps. This approach opens not only new possibilities for the bifurcation analysis, but also for the numerical treatment. Rotation solutions and POMs appear as fixed points of the Poincaré maps which may loose their stability due to Neimark-Sacker bifurcations where invariant curves bifurcate which correspond with so called quasi-POMs. If road works are not present, the Neimark-Sacker bifurcation becomes the Hopf bifurcation analysed in [GSW04], and quasi-POMs specialize to headway-periodic solutions. Our type of Poincaré maps correspond with traffic measurements on fixed positions on the road. This leads unavoidable to fundamental diagrams which typically are produced by real measurements.

The paper is organized in the following way. In section 2 we recall the known analysis for the homogeneous case with no road works. Section 3 contains the main results of this paper in the presence of road works. We introduce the concept of rotation solutions, POMs and Poincaré maps. In the latter case we exploit the cyclic symmetry of our model which justifies a symmetry adapted reduced Poincaré map. Several numerical simulations and figures, based on these maps, visualize the results. Here also macroscopic interpretations in the framework of spatio-temporal traffic flow quantities are givem. Section 4 is devoted to the fundamental diagrams for the very simple traffic models under consideration in this paper.

2. Models and analysis without road works. As in [GSW04, GSSW07], we will consider a microscopic car following model, where N cars are moving around a circular road of length L. Each car is driven according to an optimal velocity function V_j which may depend on j for individual drivers (see [BHN$^+$95]):

$$\ddot{x}_j = \frac{1}{\tau_j}(V_j(x_{j+1} - x_j) - \dot{x}_j), j = 1, ..., N, \quad x_{N+1} = x_1 + L. \tag{2.1}$$

Mostly, the so-called *homogeneous model* is considered, where V_j and τ_j do not depend on j. To model road works, our focus is on optimal velocity functions depending on the position x of the circle.

We start with a short review of the results in [GSW04, GSSW07] for (2.1) which can be written as a first order $2N$-system:

$$\left\{ \begin{array}{rcl} \dot{x}_j &=& v_j \\ \dot{v}_j &=& \frac{1}{\tau_j}(V_j(x_{j+1} - x_j) - v_j) \end{array} \right\}, \quad j = 1, \ldots, N, \quad x_{N+1} = x_1 + L. \tag{2.2}$$

It is important to distinguish $x_j(t) \in \mathbb{R}$ measuring the distance of the road, that has been covered by car j at time t and $\xi_j(t) := x_j(t) \bmod L$, denoting the position of car j on the circle. Then $x_j(t)$ contains the information about the number of the rounds, car j has passed up to time t. Setting $\mathbf{x} := (x_1, ..., x_N, v_1, ..., v_N)$, (2.2) can shortly be described by $\dot{\mathbf{x}} = f(\mathbf{x})$, an autonomous system on $\mathbb{R}^{2N}$. But it might be useful to consider (2.2) as an ODE on the manifold $(S^1_L)^N \times \mathbb{R}^N$ with the circle S^1_L of length L. Headways are denoted by $y_j := x_{j+1} - x_j$.

There exist quasi-stationary solutions of (2.1), $x^0_j(t)$, with velocities c, constant in time, equal for all drivers, and headways $d_j(c)$, constant in time, but possibly different for different drivers.

A stability analysis can be performed by replacing x_j by $x_j - x^0_j$ such that the quasi-stationary solutions become equilibrium points. Linearizing the system it turns

out that there always exists an algebraic simple eigenvalue $\lambda = 0$. Due to the quantity $\sum_{j=1}^{N} y_j = L$ this eigenvalue can be eliminated by a reduction of Eq. (2.1) to a $(2N-1)$-dimensional system in $N-1$ headways and N velocities. The stability of the quasi-stationary solutions depends on the *average density* $\frac{N}{L}$; as a variation of N would lead to completely new systems, alternatively, the length L is chosen as bifurcation parameter, and Hopf bifurcations can be numerically observed leading to periodic solutions in headways and velocities.

Much more can be stated in the homogeneous case where the optimal velocity function V and the relaxation parameter τ do not depend on j and x. Model (2.1) reads now

$$\ddot{x}_j(t) = \frac{1}{\tau}(V(x_{j+1}(t) - x_j(t)) - \dot{x}_j(t)), j = 1, ..., N, x_{N+1} = x_1 + L \tag{2.3}$$

This model is well understood, the quasi-stationary solutions are $x_j^0(t) = j \cdot L/N + tV(L/N), j = 1, 2, ..., N$, with headways L/N, velocities $c := V(L/N)$ for all cars, for all times.

A linear stability analysis shows that $V'(L/N) < \frac{1}{1+\cos(2\pi/N)}$ is the condition for asymptotic stability.

Hopf bifurcation with *wave number (mode)* k occurs if

$$V'(L/N) = \frac{1}{1 + \cos(2\pi \cdot k/N)}.$$

The corresponding Hopf-frequency is given by

$$\omega_{N,k} := \frac{\sin(2\pi \cdot k/N)}{1 + \cos(2\pi \cdot k/N)}.$$

Bifurcation of solutions with periodic headways y_j and periodic velocities $v_j = \dot{x}_j$, having asymptotic period $T := T_{N,k} := \frac{2\pi}{\omega_{N,k}}$ is a consequence of the Hopf theorem. By calculation of the first Lyapunov coefficient the quality of the Hopf bifurcation (*super-/subcritical*) can be analyzed.

The Z_N-symmetry of the ODE in the homogeneous case is characterized by the traveling wave property

$$y_j(t + kT/N) = y_{j+1}(t), j = 1, 2, ..., N, \quad v_j(t + kT/N) = v_{j+1}(t),\ j = 1, 2, ..., N.$$

The most important case is $k = 1$, when the quasi-stationary solutions loose stability.

3. Model with road works. In the case of road works the optimal velocity function additionally depends on the position $x \in S_L^1$. We introduce a real parameter $\varepsilon \geq 0$ which measures the strength of the road works. In our model, the maximal speed of car j decreases with ε and depends on position x (Fig. 3.1). The optimal velocity V_j in (2.1) and (2.2) is replaced by $V_{j,\epsilon}$ defined as

$$V_{j,\epsilon}(x, y) = \left(1 - \epsilon e^{-(x - \frac{L}{2})^2}\right) V_j(y) \tag{3.1}$$

Our aim is to perform a bifurcation analysis with respect to L and ε.

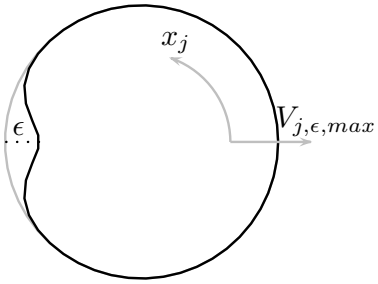

FIG. 3.1. *A region of reduced maximal optimal velocity modelling road works.*

3.1. Inhomogeneous drivers. Though most of our numerical results are performed for the homogeneous case of equal cars, part of the analysis is valid for the inhomogeneous case as well. The model (compared to (2.1)) is

$$\ddot{x}_j = \frac{1}{\tau_j}(V_{j,\varepsilon}(x_j, x_{j+1} - x_j) - \dot{x}_j), \quad j = 1, ...N, \quad x_{N+1} = x_1 + L, \tag{3.2}$$

respectively as a first order system

$$\left\{ \begin{array}{lcl} \dot{x}_j & = & v_j \\ \dot{v}_j & = & \frac{1}{\tau_j}(V_{j,\varepsilon}(x_j, x_{j+1} - x_j) - v_j) \end{array} \right\}, \quad j = 1, \ldots, N, \quad x_{N+1} = x_1 + L. \tag{3.3}$$

The main question is as follows: what kinds of solutions the quasi-stationary solutions are perturbed to by variation of the road works parameter ε from the situation without road works ($\varepsilon = 0$) to $\varepsilon > 0$?

For this aim we introduce *rotation solutions*. These are special T-periodic solutions of (3.2) being understood as a $2N$-system on the manifold $(S^1_L \times \mathbb{R})^N$.

Numerically and analytically we prefer to treat (3.3) as a $2N$-system on $\mathbb{R}^{2N}$. In this context a rotation solution with *orbital period* T and *rotation number* k is defined by

$$x_j(t + T) = x_j(t) + kL, \quad v_j(t + T) = v_j(t), \quad j = 1, 2, ..., N,$$

where T and k are assumed to be minimal. We will restrict to the special, but most important case $k = 1$.

Setting $\mathbf{\Lambda} := (L, ..., L, 0, ..., 0)$, rotation solutions are defined by

$$\mathbf{x}(t + T) = \mathbf{x}(t) + \mathbf{\Lambda} \text{ for all } t.$$

We see immediately that our quasi-stationary solutions for $\varepsilon = 0$ are rotation solutions with *orbital period* $T := L/c$, where c is the common velocity of the drivers. But observe that the headway-T-periodic solutions we get by Hopf bifurcations in general are *not* rotation solutions with orbital period T. But they always satisfy

$$x_j(t + T) = x_j(t) + L_p, j = 1, 2, ..., N$$

with an orbital length L_p. If L_p and L are commensurable, formally the headway-T-periodic solutions are rotation solutions with possibly large periods mT and rotation numbers k.

From the stability theory for periodic orbits of autonomous systems we know that each rotation solution possesses $2N$ Floquet multipliers $\mu_k, k = 1, 2, ..., 2N$ one

of which is always one due to the autonomicity of the system. The Floquet multipliers are the eigenvalues of the linearization $D\Phi^T(\mathbf{x}(t))$ of the time-T-map Φ^T at any point $\mathbf{x}(t)$ of the periodic orbit. Observe that $\Phi^T(\mathbf{x}(t)) = \mathbf{x}(t) + \mathbf{\Lambda}$ and that $\mathbf{x}(t)$ is fixed point of the map Q, defined by $Q(\mathbf{x}) := \Phi^T(\mathbf{x}) - \mathbf{\Lambda}$.

The trivial Floquet multiplier $\mu_1 = 1$ can be eliminated by introducing a Poincaré map Π wrt to a transversal section in the state space, see sec. 3.3. Then a rotation solution corresponds to a *fixed point* ξ_0 of Π, and the possibly non-trivial Floquet multipliers are the $2N-1$ eigenvalues of $D\Pi(\xi)$ which determine the orbital (asymptotic) stability of the rotation solution and possible bifurcations.

Recall, that the quasi-stationary solutions for $\varepsilon = 0$ can be considered as equilibrium points in a $2N$-system $\dot{w} = f(w)$ with $2N$ eigenvalues λ_k of $Df(0), k = 1, 2, ..., 2N$. The relation of these eigenvalues to the Floquet multipliers $\mu_k, k = 1, 2, ..., 2N$, of the quasi-stationary solutions considered as rotation solutions simply is $\mu_k = e^{\lambda_k T}, k = 1, 2, ..., 2N$. The trivial eigenvalue $\lambda_1 = 0$ corresponds to the trivial Floquet multiplier $\mu_1 = 1$.

A Hopf bifurcation, being observed in the $(2N-1)$-system of headways and velocities, appears now as a torus bifurcation where rotation solutions bifurcate to so-called *quasi-rotation solutions*. Here we follow the notion of *quasi-periodic*. In the context of Poincaré maps we encounter Neimark-Sacker bifurcations where fixed points bifurcate into invariant curves.

What happens to those solutions introducing road works ($\varepsilon > 0$)? Since, for $\varepsilon = 0$, $\lambda = 0$ is always an algebraically simple eigenvalue of $Df(0)$, the trivial Floquet multiplier $\mu = 1$ is algebraically simple, the nonlinear equation $\Pi(\xi) - \xi = 0$ has an isolated solution ξ_0, and by the Implicit Function Theorem we have fixed points $\xi(\varepsilon)$ of Π which correspond to rotation solutions with orbital period $T(\varepsilon)$. We state:

THEOREM 3.1. *For fixed L, there is an $\varepsilon_0 > 0$ such that (3.2) admits rotation solutions $\mathbf{x}(\varepsilon, t)$ for $0 \le \varepsilon < \varepsilon_0$ with orbital period $T(\varepsilon)$ which coincide for $\varepsilon = 0$ with the quasi-stationary solution ($\mathbf{x}(0,t) = x^0(t)$) and depend smoothly on ε.*

If the quasi-stationary solution $\mathbf{x}^0$ is asymptotically stable (unstable), the rotation solutions are orbital asymptotically stable (unstable).

REMARK 1. *For $\varepsilon = 0$ two Hopf-points (for certain critical L) may separate stable and unstable quasi-stationary solutions. Hence it can be expected that an analogue situation holds for the rotation solutions. With more sophisticated methods using regular defining equations for Neimark-Sacker bifurcation points (see [Kuz98]) the following holds:*

If the quasi-stationary solution is non-hyperbolic due to a Hopf bifurcation (wrt L) in the (L, ε)-plane there is a curve of Neimark-Sacker bifurcation points emanating in the Hopf point for $\varepsilon = 0$.

More precisely: For small $\varepsilon > 0$, there is an $L = L(\varepsilon)$ such that (3.2) admits a non-hyperbolic rotation solution, and there are L close to $L(\varepsilon)$ such that there exist (bifurcate) closed invariant curves of the Poincaré map Π which correspond with quasi-rotation solutions.

Thm. 3.1 and the succeeding Remark 1 are in analogy to an autonomous system with Hopf bifurcation and a periodical forcing with strength ε, see [KMR92]. Here hyperbolic equilibria are perturbed to periodic solutions, and periodic solutions of the autonomous system are perturbed to quasi-periodic solutions. A Hopf bifurcation point is perturbed into a curve of torus bifurcation points in the (L, ε)-plane.

3.2. Homogeneous drivers. Now we consider the road works model where the drivers of the cars obey the same velocity law. We will make Thm. 3.1 more detailed

wrt the underlying Z_N-symmetry. The ODE system is given by

$$\left\{ \begin{array}{lcl} \dot{x}_j & = & v_j \\ \dot{v}_j & = & \frac{1}{\tau}(V_\varepsilon(x_j, x_{j+1} - x_j) - v_j) \end{array} \right\}, \quad j = 1, \ldots, N, \quad x_{N+1} = x_1 + L. \quad (3.4)$$

We will show that the rotation solutions we obtain by Thm. 3.1 have a special Z_N-symmetry, defined by

Definition: A rotation solution with orbital period T (defined by $\mathbf{x}(t+T) = \mathbf{x}(t) + \mathbf{\Lambda}$) is called a *Ponies-On-A-Merry-Go-Round-solution* (see [AGMP91], shortly called a *POM*), if

$$x_j(t + T/N) = x_{j+1}(t) \text{ for all } t,\ j = 1, 2, ..., N.$$

This corresponds with the Z_N-symmetry of the Hopf-periodic solutions for $\varepsilon = 0$, mentioned in the Introduction.

Now we are going to exploit this symmetry in more details:

Let

$$S_+(x_1, ..., x_N, v_1, ..., v_N) := (x_2, x_3, ..., x_N, x_1 + L, v_2, v_3, ..., v_N, v_1)$$

be the forward shift of the car constellation on the circle. S_+ is affine linear. Calling the linear part C_+, we have $C_+(\xi_1, ..., \xi_N, v_1, ..., v_N) := (\xi_2, \xi_3, ..., \xi_N, \xi_1, v_2, v_3, ..., v_N, v_1)$.

It can be easily shown that the flow Φ^t of (3.4) is S_+-equivariant, since $S_+ \circ \Phi^t = \Phi^t \circ S_+$ for all t.

This can be understood as follows: Starting the dynamics with state $\mathbf{x}$ and performing a forward shift after time t or changing the initial state $\mathbf{x}$ by a forward shift and letting t time units pass — the final state is the same.

The equivariance of the vector field f of (3.4) can be described as

$$f \circ S_+ = DS_+ \circ f,$$

where the differential $DS_+ = C_+$ is the linear part of S_+.

C_+ generates the cyclic group Z_N since $C_+^N = I$ or $S_+^N(\mathbf{x}) = \mathbf{x} + \mathbf{\Lambda}$ (where $\mathbf{\Lambda} = (L, ..., L, 0, ..., 0)$). Now it turns out that a POM is Z_N-invariant in the sense that $S_+(\mathbf{x}(t)) = \mathbf{x}(t + T/N)$ for all t.

Having POMs $\mathbf{x}(t)$ with orbital period T we consider the (reduced) time-T/N-map Φ^α with $\alpha := T/N$ and define

$$P(\mathbf{x}) := S_-(\Phi^\alpha(\mathbf{x}))$$

with the backward shift $S_- := (S_+)^{-1}$ or equivalently by

$$P(\mathbf{x}) := C_-(\Phi^\alpha(\mathbf{x})) - (L, 0, \ldots, 0),$$

where C_- is the inverse of C_+.

Then every $\mathbf{x}_0 = \mathbf{x}(t)$ is a fixed point of P since $S_+(\mathbf{x}_0) = \Phi^\alpha(\mathbf{x}_0)$ holds. Obviously the following holds: $S_-^N(\mathbf{x}) = \mathbf{x} - \mathbf{\Lambda}$ for all $\mathbf{x}$, $P^N = Q$, where $Q(\mathbf{x}) = \Phi^T(\mathbf{x}) - \mathbf{\Lambda}$, $\mathbf{x}_0$ is fixed point of Q, and the eigenvalues of $DQ(\mathbf{x}_0)$ are the Floquet multipliers of the POM. These can be obtained by the eigenvalues of $DP(\mathbf{x}_0)$ taken to the Nth power.

REMARK 2. *Treating (3.4) as an ODE on the manifold $(S_L^1)^N \times \mathbb{R}^N$ (an N-dimensional cylinder), the Z_N-equivariance properties can simply described by*

$C_+(f(\mathbf{x})) = f(C_+(\mathbf{x}))$ *for the vectorfield and* $C_+ \circ \Phi = \Phi \circ C_+$ *for the flow* Φ*, since* $C_+^N = I$*. In this setting, POMs with orbital period* T *are* T*-periodic solutions with orbital* Z_N*-symmetrie.*

In the following Sec. 3.3 we will present a corresponding construction, replacing Q by a Poincaré-map and P by a reduced Poincaré-map to eliminate the trivial Floquet multiplier $\mu := 1$ of a POM.

3.3. Poincaré maps. We assume that we have a rotation solution $\mathbf{x}(t)$. A suitable Poincaré-section is given by $\Sigma := \{\mathbf{x} : x_1 \bmod L = 0\}$ which (in the state space $\mathbb{R}^{2N}$) consists of an infinite number of parallel sections $\Sigma^n := \{\mathbf{x} : x_1 = nL\}, n \in \mathbb{Z}$. Assume that $\mathbf{x}_0 := \mathbf{x}(0) \in \Sigma$. Then $\mathbf{x}(nT) \in \Sigma$ for all $n \in \mathbb{N}$. There is a map $\hat{\Pi}$ from Σ^n to Σ^{n+1}. More precisely, $\hat{\Pi}$ maps a neighborhood of $\mathbf{x}(nT) \in \Sigma^n$ into a neighborhood of $\mathbf{x}((n+1)T) \in \Sigma^{n+1}$. The Poincaré map is defined by $\Pi(\mathbf{x}) := \hat{\Pi}(\mathbf{x}) - \mathbf{\Lambda}$, where Π maps Σ^0 into itself, and it may be assumed that $\mathbf{x}_0 := \mathbf{x}(0) \in \Sigma$ is a fixed point of Π. The return time of $\mathbf{x}_0$ wrt Π is the orbital period T.

Now let $\mathbf{x}(t)$ be a POM. There is a powerful way to reduce the complexity due to the Z_N-symmetry by introducing a *reduced Poincaré map* π: For this end we set $\Sigma' := \{\mathbf{x} : x_N \bmod L = 0\}$. Then there is a map $\hat{\pi}$ which maps a neighborhood of $\mathbf{x}(0) \in \Sigma$ to a neighborhood of $\mathbf{x}(T/N) \in \Sigma'$. The transfer time is the time passed between the state $\mathbf{x}(0)$ where car 1 is located in $x_1 = 0$ and the state where car N behind has reached the same position as car 1 before. We define the *reduced Poincaré map* π by $\hat{\pi}$ followed by a backward shift,

$$\pi(\mathbf{x}) := S_-(\hat{\pi}(\mathbf{x})) = C_-(\hat{\pi}(\mathbf{x})) - \ell.$$

Then $\mathbf{x}(0) = \mathbf{x}_0$ is a fixed point of π with return time T/N. Observe that this construction is in full analogy to that of the time T-map Q and of the reduced map P in the section before. Again we have $\pi^N = \Pi$. The eigenvalues of $D\Pi(\mathbf{x}_0)$ are the $(2N-1)$ Floquet multipliers of the POM except $\mu = 1$. These can be obtained by the eigenvalues of $D\pi(\mathbf{x}_0)$ taken to the Nth power.

Based on the reduced Poincaré map π instead of the Poincaré map Π, Thm. 3.1 can be refined and stated as follows.

THEOREM 3.2. *For fixed* L*, there is an* $\varepsilon_0 > 0$ *such that (3.4) admits POMs* $x(\varepsilon, t)$ *for* $0 \le \varepsilon < \varepsilon_0$ *with orbital period* $T(\varepsilon)$ *which coincide for* $\varepsilon = 0$ *with the quasi-stationary solution* $\mathbf{x}^0$ *and depend smoothly on* ε*.*

If the quasi-stationary solution is asymptotically stable (unstable), the POMs are orbital asymptotically stable (unstable).

REMARK 3. *As in Remark 1 it can be shown:*

If the quasi-stationary solution is non-hyperbolic due to a Hopf bifurcation (wrt L*), in the* (L, ε)*-plane, there is a curve of Neimark-Sacker bifurcation points emanating in the Hopf point for* $\varepsilon = 0$*.*

More precisely: For small $\varepsilon > 0$*, there is an* $L = L(\varepsilon)$ *such that (3.4) admits a non-hyperbolic POM, and there are* L *close to* $L(\varepsilon)$ *such that there exist (bifurcate) closed invariant curves of the reduced Poincaré map* π *(see Fig. 3.2). These correspond with closed invariant curves of the Poicaré map* Π*. We call the quasi-rotations mentioned in Remark 1 quasi-POMs. If the Hopf bifurcation point for* $\varepsilon = 0$ *is supercritical we expect the same for the Neimark-Sacker bifurcation points for small* $\varepsilon > 0$*. In this case we will encounter stable quasi-POMs.*

3.4. Numerics. The presented approach via Poincaré maps or reduced Poincaré maps can be used immediately as a numerical tool to calculate the solutions. Especially in the homogeneous case there is an efficient way to compute POMs by solving

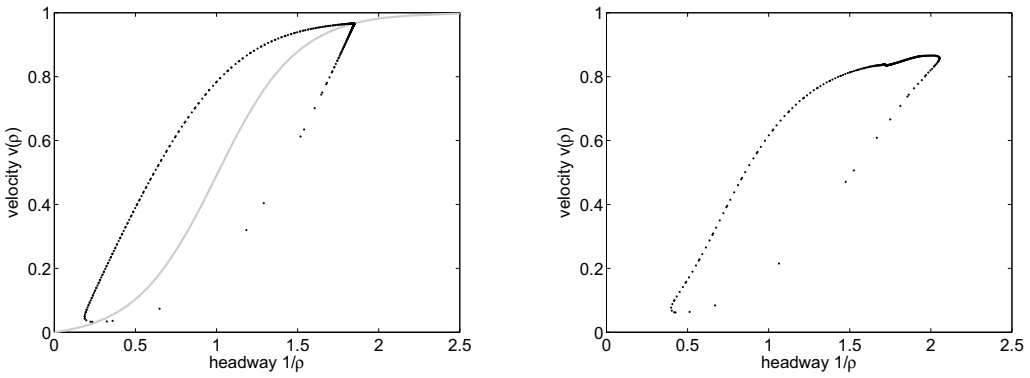

(a) $N = 10, L = 12, \epsilon = 0$ (b) $N = 10, L = 12, \epsilon = 0.2$

FIG. 3.2. *Two closed invariant curves of the reduced Poincaré map π. On the left also the optimal velocity function V_0 is given in gray.*

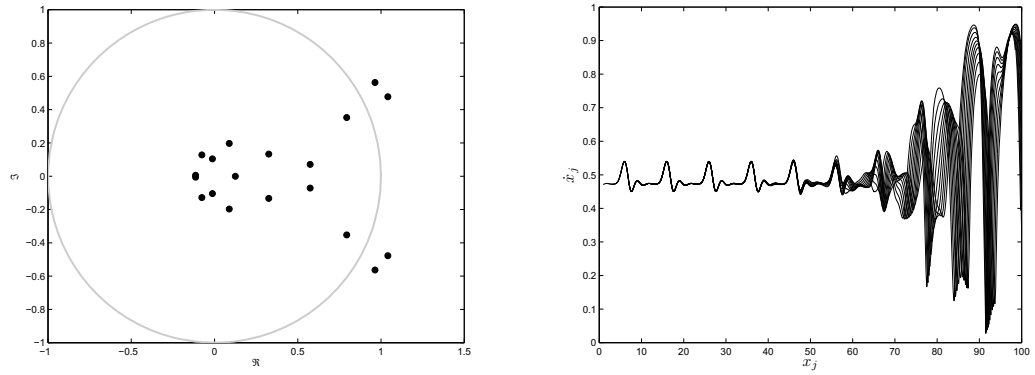

FIG. 3.3. *An unstable POM with corresponding Floquet multipliers (left) for $N = 10, L = 10, V_{max} = 1, \epsilon = 0.1$.*

the fixed point equation $\xi = \pi(\xi)$ for the reduced Poincaré map π. Remember that the corresponding Floquet multipliers are just the eigenvalues of $D\pi(\xi)$ taken to the power N. Hence, for the stability analysis, it is sufficient to compute these eigenvalues, particularely, since they are better separated than the Floquet multipliers. We call them *r*educed Floquet multipliers.

In this section we choose the optimal velocity function

$$V(x) = \frac{\tanh 2(x-1) + \tanh 2}{1 + \tanh 2}, \tag{3.5}$$

suggested by [BHN$^+$95], and we set the driver's reaction time to $\tau = 1$.

Fig. 3.3 (left) shows the reduced Floquet multipliers for special parameters with a corresponding unstable POM. On the right side a simulation is shown starting close to an unstable POM and converging to a quasi-POM.

For each fixed $\varepsilon > 0$, it is a classical task to perform a numerical continuation of the POMs wrt the bifurcation parameter L, based on the reduced Poincaré map π. As a by-product we obtain the reduced Floquet multipliers and are able to localize Neimark-Sacker bifurcations for $L = L(\varepsilon)$ characterized by a pair of complex conjugate reduced Floquet multipliers of modulus one. By this we get a numerical approximation

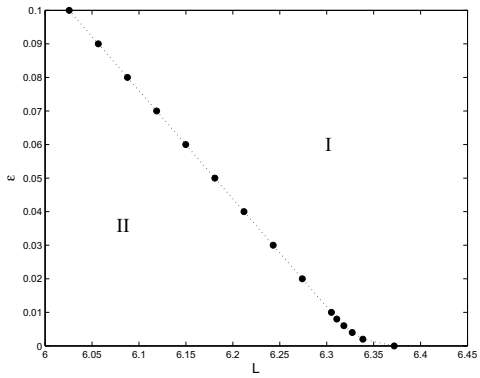

FIG. 3.4. *A curve of Neimark-Sacker bifurcations in the (L, ϵ)-plane for $N = 5$.*

ϵ	I	II
0	trivial POM x^0	Hopf periodic solution
> 0	POM x^ϵ	quasi-POM

TABLE 3.1
Four different attractors.

of the Neimark-Sacker curve, mentioned in Remark 3, exemplarily shown for the case $N = 5$ in Fig. 3.4. The bifurcation takes place for decreasing L, hence on its right (region I) there are stable, on the left (region II) unstable POMs and stable quasi-POMs (assuming that the Hopf bifurcation for $\varepsilon = 0$ is supercritical). The curve starts for $\varepsilon = 0$ in a supercritical Hopf point ($L \approx 6.37$).

In the following we discuss four different showcase scenarios in the (L, ϵ)-parameter plane; using the same I-II-notation as in Fig. 3.4, Table 3.1 explains the character of the attractive solutions presented in Figs. 3.5 and 3.6.

The POMs have a simple structure from the traffic point of view. The main influence for each car is given by the road works, not by the cars in front. The velocity of each car depends only on its position on the circle. Fig. 3.5(c) shows a typical picture of an attractive POM in relation to the maximal velocity $V_{\varepsilon,max}$ (grey). In comparison see Fig. 3.5(a) for the trivial POM x^0.

It is much more difficult to reveal the traffic structure of quasi-POMs. To study the influnece of the average density N/L on the dynamics we reduce L to reach the unstable region (II) behind the Neimarck-Sacker bifurcation (for $N = 10$ the critical length is $L_H \approx 14.12$). Fig. 3.5(d) shows a typical phase curve of a car (here car No.1). Small velocities (peaks down) can be interpreted as traffic jams. Two periods seem to be present. From the scenario without road works (Fig. 3.5(b)) we guess that the small period is due to the Hopf-periodic rotating wave dynamics for $\varepsilon = 0$ and that the large period is caused by the road works. The smallest velocities occur when road works and traffic jam of the rotating wave coincide.

We can define macroscopical functions like velocity $v(\xi, t)$, density $\varrho(\xi, t)$, and flow $q(\xi, t) := v(\xi, t) \cdot \varrho(\xi, t)$ for such (ξ, t) for which there is a car (of number j) with $\xi = x_j(t) \bmod L$. For density we take the inverse of the headway. Colorizing the trajectories $\{(x_j(t) \bmod L, t), t \geq 0\}$ according to the macroscopic values we optain pictures as in Fig. 3.6(a)-3.6(d).

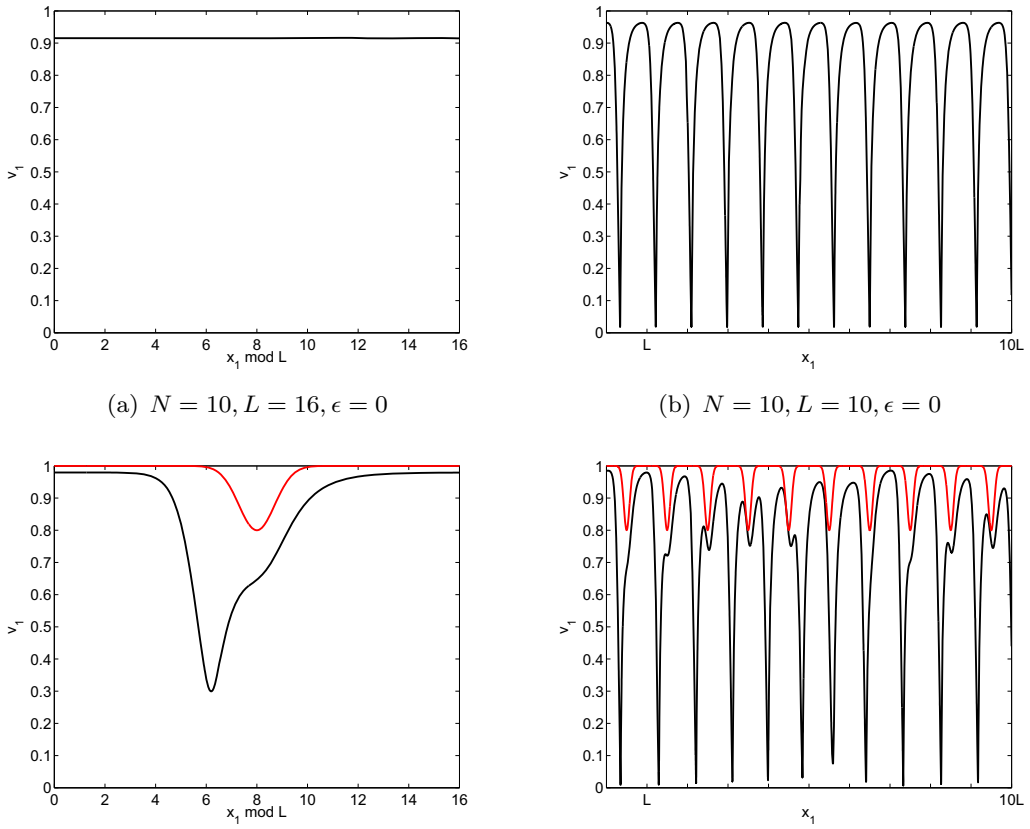

(a) $N = 10, L = 16, \epsilon = 0$

(b) $N = 10, L = 10, \epsilon = 0$

(c) $N = 10, L = 16, \epsilon = 0.2$

(d) $N = 10, L = 10, \epsilon = 0.2$

FIG. 3.5. *Four different scenarios according to Fig. 3.4 and Table 3.1.*

Mathematically, it is fascinating to visualize quasi-POMs by invariant (closed) curves in the Poincaré section. These curves can be interpreted as follows: At a fixed position on the circle, each time, when a car passes this position, there is a stroboscopic view on the whole traffic. For the case of an unstable fixed point of π see Fig. 3.7 where the quasi-POM is represented by five closed limit curves. Recognize the lightblue (1-dimensional) closed invariant line on the left marking the fixed position on the circle, where stroboscope is switched on by the passing cars.

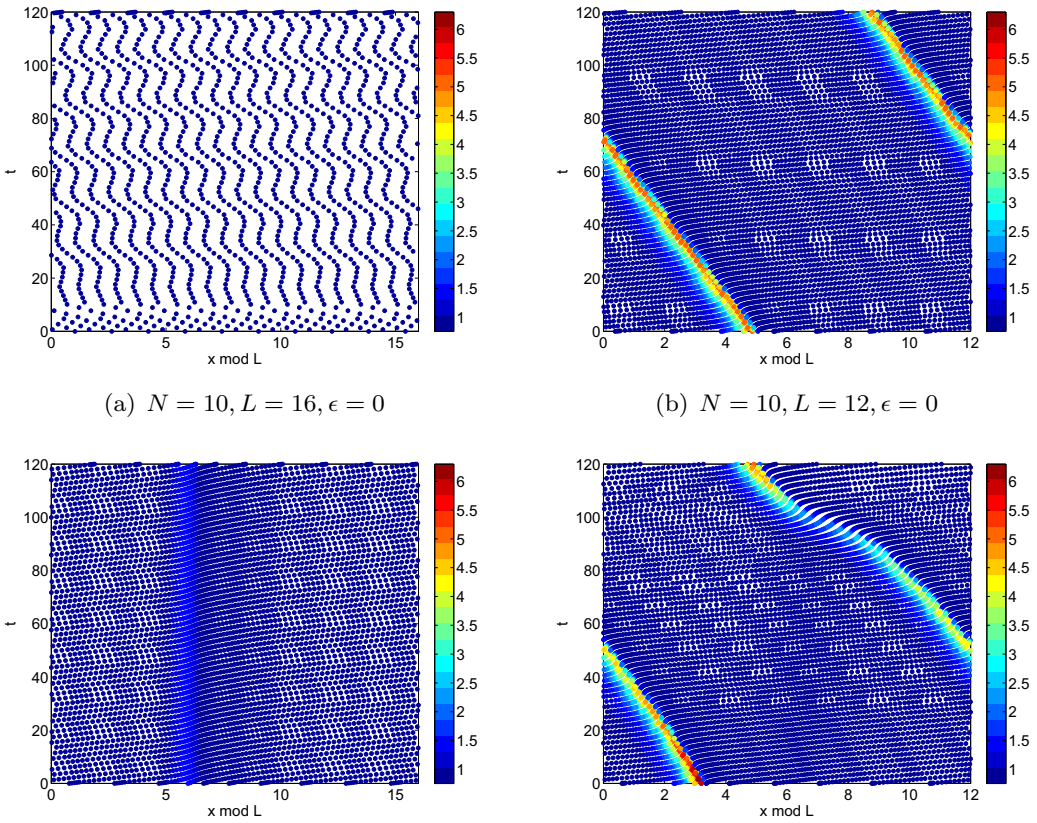

(a) $N = 10, L = 16, \epsilon = 0$

(b) $N = 10, L = 12, \epsilon = 0$

(c) $N = 10, L = 16, \epsilon = 0.2$

(d) $N = 10, L = 12, \epsilon = 0.2$

FIG. 3.6. *Macroscopic perspectives of a microscopic modell according to Fig. 3.5.*

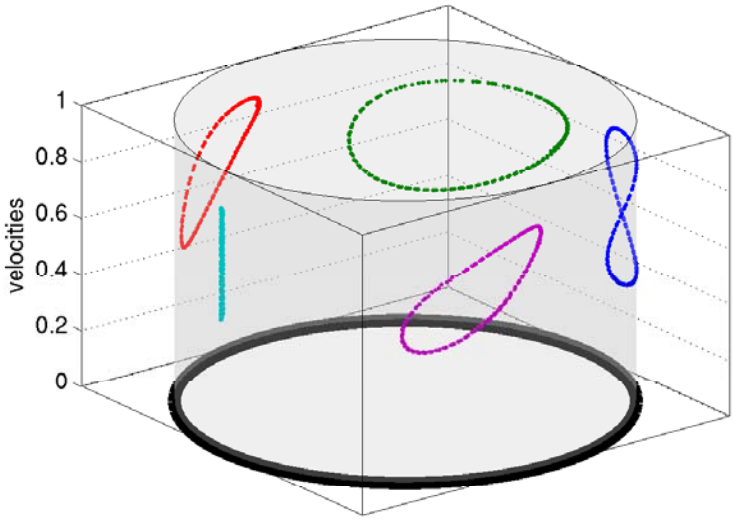

FIG. 3.7. *A real world point of view on the reduced Poincaré map π for $N = 5, \epsilon = 0$.*

4. Fundamental diagrams. In the previous section we have seen various numerical simulation on the complex dynamical behaviour of the cars in the (very simple) traffic flow model with and without road works. The model gives the full information on the dynamics. In this section we go further with numerical simulations. We plan to bridge the gap between numerical simulations and real world traffic behaviour.

It is our aim to compare the dynamics of the previous section to real world traffic data. Real world data are obtained by measurements and can be found in the literature. There is a big variety of methods of measurement, from simple counting to fixed electronic measurement devices on the roads. However, from the literature it is not always clear how precisely the measurement was performed. E.g., in view of oscillating behaviour it would be important to know about the length of the counting intervals etc. In addition not the complete set of datas are presented. The presented traffic datas or curves are already an elaboration with respect to a certain theory, a model or a conjecture.

A very common presentation of traffic flow behaviour are fundamental diagrams. A fundamental diagram is a traffic density versus traffic flow diagram. In the very simple case of stationary traffic the flow is known to be a function of the density. At vanishing density and at maximum density the velocity (and therefore the flow) vanishes. Between these two density values there is one density value with maximal flow. For general traffic flow there cannot be expected a functional relation between flow and density. However, for low density a functional (monoton increasing) flow-density relation is known. For higher density the flow splits into two branches such that the flow-density relation takes the form of an inverted greek λ. In some cases the flow values in between these two flow branches seem also to be assumed (at least partially). At this point we remember the difficulty described above that for many fundamental diagrams in the literature we do not exactly know which data where used and how the data where put into the diagram.

The mentioned problems give rise to an (somehow inverted) alternative approach to fundamental diagrams. We try to understand which fundamental diagrams can be obtained from the (very simple) model of this paper. Therefore we use the models and the results from above and mimic different measurement methods by evaluating the reduced Poincarè map π or by following one car at equidistant time steps. For these different methods we show the corresponding fundamental diagram. As far as Hopf periodic solutions ($\epsilon = 1$) or quasi-POMs ($\epsilon > 0$) occur we encounter closed invariant curves. Measuring at a fixed position x^m means (the superscript m stays for measurement) that whenever a car passes position x^m we get a density and a flow value, i.e. we get a sequence of times $t_j^m, j = 1, ..., l$ with $x_i(t_j^m) = x^m$ for some $i = 1, ..., n$. We define - as in the previous section - the density value as the inverse of the distance to the car in front. The flow value is defined as the product of density and the velocity of the car.

$$\varrho_j = \varrho(x^m, t_j^m) = \frac{1}{x_{i+1}(t_j^m) - x^m}, \quad q_j = q(x^m, t_j^m) = \varrho(x^m, t_j^m)\dot{x}_i(t_j^m), \quad j = 1, ..., l. \tag{4.1}$$

This definition is one possible choice. However we believe that in a "continuum limit" (say for a fixed average density $\frac{N}{L}$ and number of cars $N \to \infty$) we obtain (what in the macroscopic traffic flow modelling world is called) a traffic density and a traffic flow, i.e. two functions in space and in time.

Note that we should distinguish in our fundamental diagram considerations between the "classical" case with no roadwork and the non standard case with roadwork.

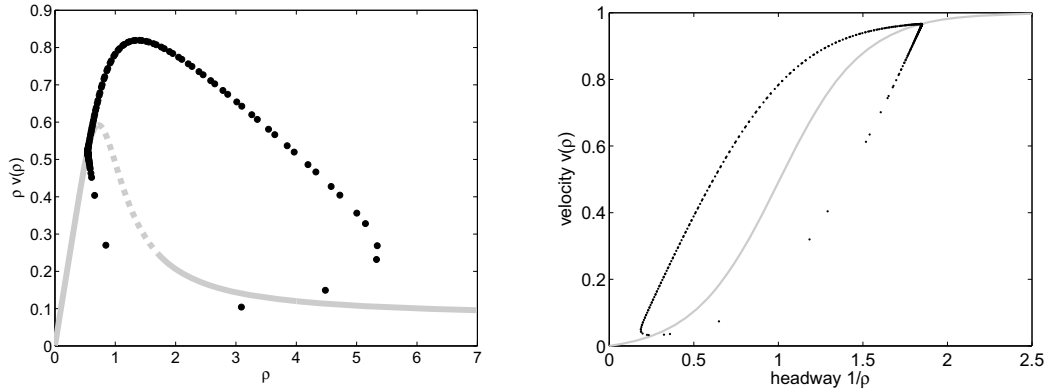

FIG. 4.1. *Fundamental diagram for $N = 10, L = 12$ measuring at a fixed point. As a reference the trivial fundamental diagram for equilibrium solutions in gray.*

The first case reflects the perfect setting for a measurement whereas the second case stays for a situation with more (known or unkonwn) influences. It makes sense to consider both cases since in real world measurement one has to face both optimal and less optimal measurement settings, positions and conditions. However, in the following we will mainly focus on the case with no road works. At the end we discuss shortly the case with road works.

We start measuring in the most intutitive way. We measure the traffic flow at one fixed position on the circular road. For the case $N = 10$, $L = 12$ we show the sequence of values $(\varrho_j, q_j), j = 1, .., 150$ for the case of a Hopf periodic solution (Fig. 4.1). The left side is the fundamental diagram. In the background we see the fundamental diagram for the quasi-stationary solution (which is unstable—dotted—in this parameter regime and will not be approached). This background diagram is the most trivial fundamental diagram corresponding to the quasi-stationary solution where all cars drive (allways) with the (desired) equilibrium velocity. The right side presents the same data but in a headway versus velocity diagram.

In reality we expect different density regimes over a measurement period. Therefore, as an experiment we mix up different diagrams for a large density interval ($N = 10$, $L = 50, ..., 4$) and obtain in the "sum" Fig. 4.2. The upper left figure ist the fundamental diagram, the upper right figure a blow up of the interesting part in the fundamental diagram and the lower figure is again the corresponding headway versus velocity diagram. Now the inverse lambda structure is obvious. Note that there ist no trivial fundamental diagram depicted in the background. The unstable regime of the quasi-stationary solutions lies between

$$L_H^1 \approx 14.1 > L > 5.9 \approx L_H^2,$$

where the subscript H is due to the critical size of L in the Hopf bifurcation. In this regime we encounter stable periodic solutions. In the low density area (below $\varrho = \frac{10}{14.1} \approx 0.71$) the quasi-stationary solutions are stable and the corresponding points in the density-flow diagram lie on the (trivial) density-flow curve. Same holds for high densities (above $\varrho = \frac{10}{5.9} \approx 1.69$). For $L_H^1 > L > L_H^2$ the (stable) periodic solutions cover a bigger density regime. Clearly they assume also density values below $\varrho = \frac{10}{L_H^1}$ and above $\varrho = \frac{10}{L_H^2}$. What is surprising is the good correspondence of the periodic solutions for different average densities $\frac{N}{L}$ especially in the low density part

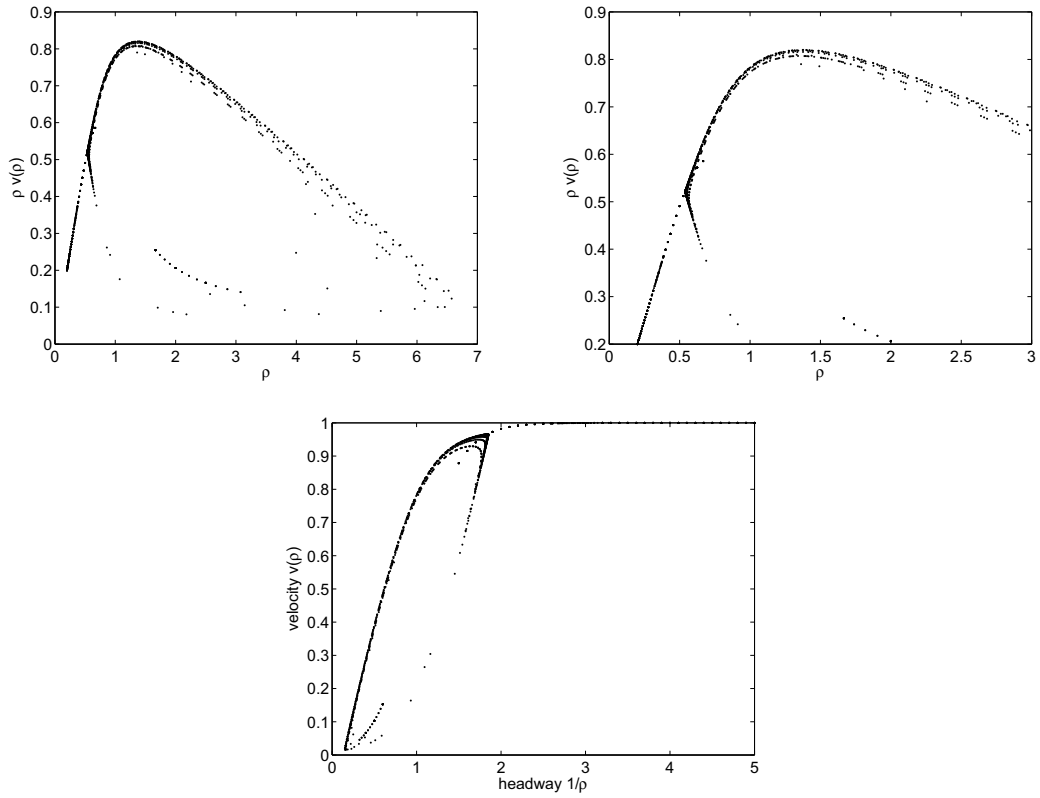

FIG. 4.2. *Overlapped fundamental diagrams for* $N = 10, L = 50, ..., 4$ *measuring at a fixed point.*

where the two branches start to coincide. There the striking part of the inverse lambda structure is formed. It seems that this type of fundamental diagrams is very robust with respect to changes in density. At the moment we have no particular explanation for this phenomenon.

We would like to mention a third method for representing traffic data in fundamental diagrams. Suppose we only count at a fixed point and that the counting interval is large. Then we obtain for every L one single (averaged) flow value. Repeating this for a large range in L (say from $L = 50, ..., 4$) we obtain a fundamental diagram. This represents time-averaged flow versus average density $\frac{N}{L}$. Note that the average density $\frac{N}{L}$ is in general not equal to the mean density over a period of the periodic solution. By simply counting the cars over a certain time period we are not able to obtain this mean density over a period in case of the periodic solution. However, the result of this third method to measure is shown in Fig. 4.3. The right figure is a blow up of the interesting detail in the left figure. Note that this is a bifurcation diagram. In the region of stable quasi-stationary solutions we have the known curve. In addition we have stable periodic solutions not only in the region where the quasi-stationary solutions are unstable. In this measuring procedure these stable periodic solutions are represented by a single value. It is very interesting to note that there is a region in $\frac{N}{L}$ (around $\frac{N}{L} = 1.5$) where the averaged flow of the periodic solutions is higher then the flow corresponding to the (unstable) quasi-stationary flow.

Let us mention an additional way of looking at the data. Sometimes in literature measurements at different points of the circular road are mixed up (see e.g. [SM06]). This leads to the idea of observing the data from the viewpoint of a single car: we

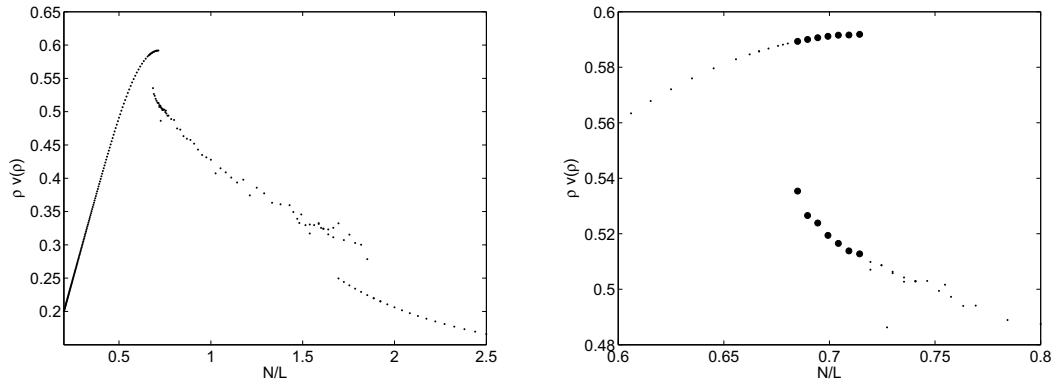

FIG. 4.3. *Fundamental diagram of time-averaged flow versus average density for* $N = 10, L = 50 \ldots 4$,

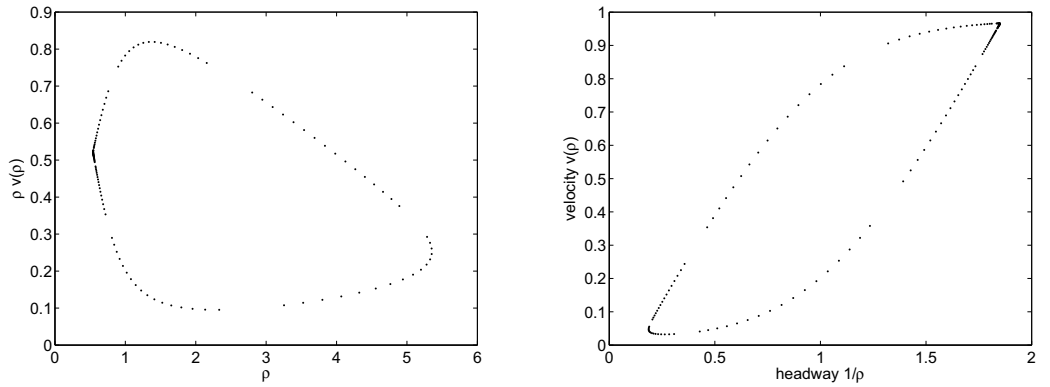

FIG. 4.4. *Fundamental diagram for* $N = 10, L = 12$ *from the viewpoint of a single car. Note the difference to figure 4.1*

take the density and the flow value of a certain fixed car by equidistant timesteps. Having a look at the corresponding fundamental diagram (see Fig. 4.4) we realise that this is almost identical to Fig. 4.1. The difference lies in how dense the points are located on the same underlying invariant curve. For this consideration the right pictures (velocity over headway) in the two figures are more adequate. At a fixed measuring point almost two-thirds of the cars are passing with low density and high velocities (Fig. 4.1, right). On the other hand, from the viewpoint of a single car the situation is different. In the right side of Fig. 4.4 we see that a single car "lives" most of the time in two extrem density-flow situation: low density with high velocities or high density with low velocities. If we define this last situation on the invariant curve as traffic jam, then the measurement corresponding to Fig. 4.4 is more suitable to recognize traffic jams.

Finally we switch to the case with road works. A main question we are interested in is the behavior of the inverted λ structure with respect to changes in ϵ. For this purpose we redo the simulations corresponding to Fig. 4.2 (upper left picture) for $\epsilon = 0.1$. The result is given in Fig. 4.5. It is interesting to note, that the main phenomena are preserved. Even in the case of road works the basic inverse lambda structure remains the dominant picture.

Regarding the solutions itselves note that the curve in Fig. 4.4 (right) becomes a

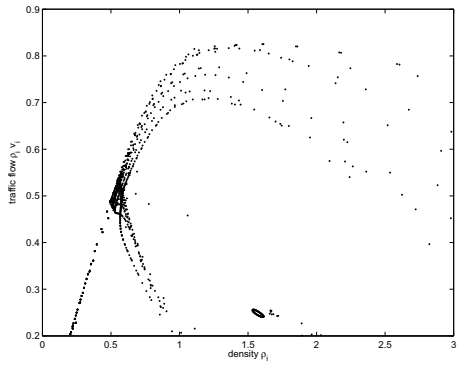

FIG. 4.5. *Overlapped fundamental diagrams for* $N = 10, L = 50, ..., 4, \quad \epsilon = 0.1$ *measuring at a fixed point.*

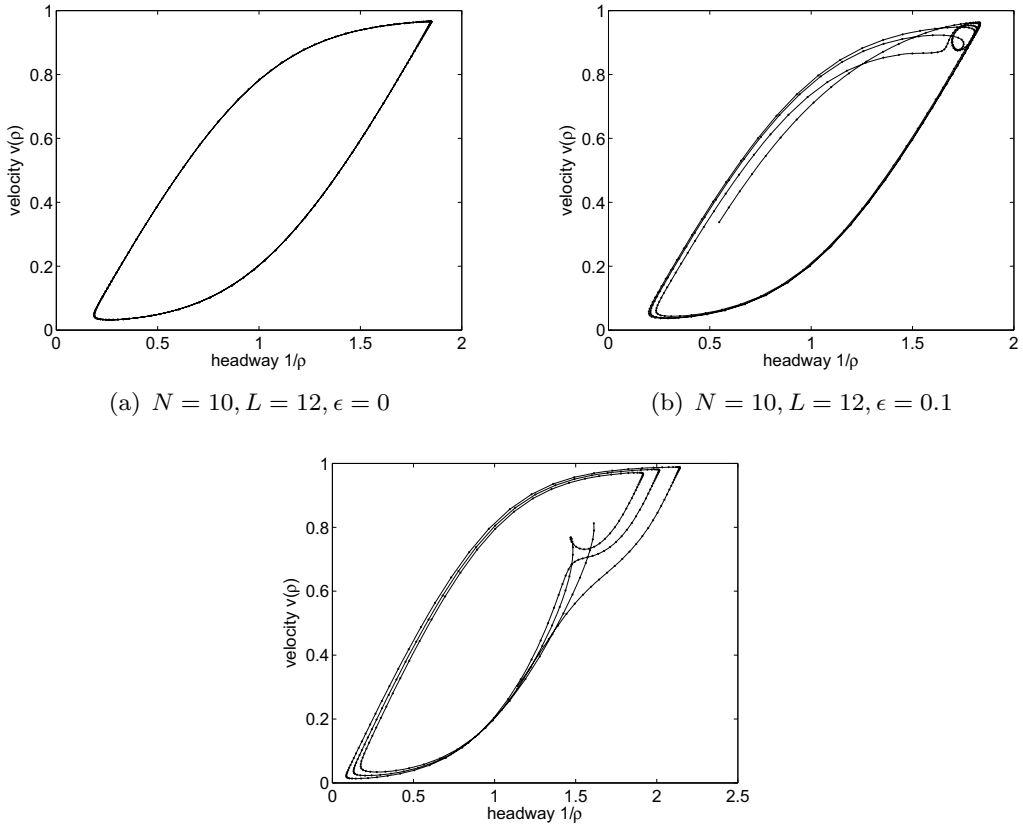

(a) $N = 10, L = 12, \epsilon = 0$

(b) $N = 10, L = 12, \epsilon = 0.1$

(c) $N = 10, L = 12, \epsilon = 0.2$

FIG. 4.6. *Fundamental diagrams from the viewpoint of a single car with equidistant (very small) timesteps with and without road works. Compare to 4.4 (right).*

limit cycle when time runs continuously (Fig. 4.6(a)). Introducing roadworks ($\epsilon > 0$) this limit cycle ($\epsilon = 0$) is smeared out to phase curves shown in Fig. 4.6(b) and Fig. 4.6(c). In the latter case the structure of quasi-POM's is not visible. This is in contrast to the stroboscopic Poincaré-view in Fig. 3.2(b) showing (a projection of) the invariant curve.

5. Conclusions. We analyse the dynamics of the classical optimal velocity model for the case of inhomogeneous drivers and for the case of road works using a new viewpoint. We believe that this viewpoint based on the study of the underlying Poincaré maps offers a powerful tool to study such non-homogeneous traffic models both analytically and numerically. In addition this approach has the advantage that it is very close to what we define as a measurement. Therefore fundamental daigrams etc. are obtained with almost no additional effort.

REFERENCES

[AGMP91] D. G. Aronson, M. Golubitsky, and J. Mallet-Paret. Ponies on a merry-go-round in large arrays of josephson junctions. *Nonlinearity*, 4:903–910, 1991.

[AKMR02] A. Aw, A. Klar, T. Materne, and M. Rascle. Derivation of continuum traffic models from microscopic follow-the-leader models. *SIAM J. Appl. Math.*, 63 (1):259–278, 2002.

[AR00] A. Aw and M. Rascle. Resurrection of 'second order' models of traffic flow. *SIAM J. Appl. Math.*, 60:916–938, 2000.

[BHN+95] M. Bando, K. Hasebe, A. Nakayama, A. Shibata, and Y. Sugiyama. Dynamical model of traffic congestion and numerical simulation. *Phys. Rev. E*, 51:1035ff, 1995.

[BM00] M. Brackstone and M. McDonnald. Car following: a historical review. *Transp. Res. F*, 2:181, 2000.

[Gre04] J. M. Greenberg. Congestion redux. *SIAM J. Appl. Math.*, 64 (4):1175–1185, 2004.

[GSSW07] I. Gasser, T. Seidel, G. Sirito, and B. Werner. Bifurcation analysis of a class of 'car following' traffic models ii: Variable reaction times and aggressive drivers. *Bulletin of the Institute of Mathematics, Academia Sinica*, 2(2), 2007.

[GSW04] I. Gasser, G. Sirito, and B. Werner. Bifurcation analysis of a class of 'car following' traffic models. *Physica D*, 197/3-4:222–241, 2004.

[Hel01] D. Helbing. Traffic and related self-driven many-particle systems. *Rev. Modern Phys.*, 73:1067–1141, 2001.

[KMR92] Yu. A. Kuznetsov, S. Muratori, and S. Rinaldi. Bifurcations and chaos in a periodic predator-prey model. *International Journal of Bifurcation and Chaos*, 2 (1):117–128, 1992.

[Kuz98] Y. A. Kuznetsov. *Elements of Applied Bifurcation Theory.*, volume 112 of *Applied Mathematical Sciences*. Springer, 1998.

[KW04] A. Klar and R. Wegener. *Traffic flow: models and numerics*. Birkhaeuser, 2004. Editors: P. Degond, L. Pareschi, G. Russo.

[LW55] M. J. Lighthill and G. B. Whitham. On kinematic waves: Ii. a theory of traffic on long crowded roads. *Proc. R. Soc.*, A 229:317–345, 1955.

[NWW03] K. Nagel, P. Wagner, and R. Woesler. Still flowing: approaches to traffic flow and traffic jam modeling. *Operations Research*, 51(5):681–710, 2003.

[OKW05] G. Orosz, B. Krauskopf, and R. E. Wilson. Bifurcations and multiple traffic jams in a car-following model with reaction-time delay. *Physica D*, 211:277–293, 2005.

[OS06] G. Orosz and G. Stépán. Subcritical hopf bifurcations in a car-following model with reaction-time delay. *Proc. R. Soc.*, 462:2643–2670, 2006.

[OWK04] G. Orosz, R. E. Wilson, and B. Krauskopf. Global bifurcation investigation of an optimal velocity traffic model with driver reaction time. *Phys. Rev. E*, 70:1–10, 2004.

[SM06] F. Siebel and W. Mauser. On the fundamental diagram of traffic flow. *SIAM J. Appl. Math.*, 66 (4):1150–1162, 2006.

[SS93] A. Schadschneider and M. Schreckenberg. Cellular automaton models and traffic flow. *J. Physics A: Math. Gen.*, 26:L679–L683, 1993.